

Chapter 24

Array Phase Shifters: Theory and Technology

Robert R. Romanofsky
Senior Technologist
Communication and Intelligent Systems Division
NASA Glenn Research Center
Cleveland, OH 44135

- 24.1 Introduction
- 24.2 Semiconductor
 - 24.2.1 High-Pass/Low-Pass
 - 24.2.2 Loaded Line
 - 24.2.3 Switched Line
 - 24.2.4 Switching Q
- 24.3 Thin Film Ferroelectric
 - 24.3.1 Materials and Basic Properties
 - 24.3.2 Coupled Microstripline
 - 24.3.3 Theory of Coupled-Line Type
- 24.4 MEMS
- 24.5 Slow-Wave
 - 24.5.1 One-Dimensional Periodic Structures
 - 24.5.2 Ferroelectric Varactor
- 24.6 Ferrite
- 24.7 Effect of Phase Shifter Behavior on Phased Array Bit Error Rate
 - 24.7.1 Modulo 2π Effects
 - 24.7.2 Phase Errors
- 24.8 Trends
 - 24.8.1 Optical Phased Arrays
 - 24.8.2 Multiferroics
 - 24.8.3 Printable Phase Shifters
- 24.9 Summary
- References

24.1 Introduction

Phase shifters are linear one- or two-port devices for adjusting the reflection or insertion carrier phase of a band-limited signal, nominally from 0 to 2π radians. A perfect phase shifter would have: no insertion loss, a voltage standing wave ratio of 1:1, arbitrarily high power handling capability, linear phase-versus-frequency response, an arbitrarily small footprint,

radiation immunity, no DC power consumption, and of course be free. Remarkably, real phase shifters can approach some of these idealized attributes. New processing techniques hold promise to significantly reduce manufacturing cost (see “Trends” at the end of this chapter).

The most prevalent use for microwave phase shifters continues to be scanning directly-radiating or “reflectarray” phased-array antennas. That market continues to be dominated by military radar and tracking platforms. Many of the arrays developed during the last four decades had production runs of over 50 and even one radar system can require a very large number of phase shifters. The S-band AEGIS/SPY-1 represents a production run of 234 systems, each with 4000 phase shifters. The Theater High Altitude Area Defense (THAAD) ground-based radar required over 60,000 MMIC phase shifter chips. That program demonstrated a per-module cost of about \$1,000.

Two provocative commercial applications are emerging: cognitive radios and the “internet-of-things.” The former provides an approach to stretch the limited electromagnetic spectrum by dynamically adapting communications systems to the electromagnetic environment. This ability necessitates agile radio front-ends, including the antenna system. An intelligent antenna uses beam-forming to optimize spatial asset connectivity and to cancel interference, and may involve frequency agility as well. The latter includes intelligent transportation and automated highway systems (e.g. adaptive cruise control, collision avoidance radar, and even “connected” cars, etc.). It has been estimated that 60 percent of rear-end collisions could be eliminated if a driver had an additional 0.5 seconds to react¹. Global sales of radar based collision avoidance sensors are expected to exceed \$4 billion by 2020². Societal implications of self-driving cars, a direction we appear to be headed in, remain to be seen. A third burgeoning market for electronically steered phased array antenna systems is commercial aircraft satellite communications to facilitate live

television reception as well as business data. The phased array offers an agile, aerodynamic solution to compensate for pitch, yaw and roll maneuvers and maintain an optimal link to a geostationary satellite.

Real phase shifters have consequential effects on communications system performance and economics. Evolving high data rate communications systems demand greater attention to subtle aspects of information theory and electromagnetic engineering. As the ratio of signaling bandwidth to carrier frequency decreases, less familiar phenomenon can influence system performance. And, new coding techniques are pushing channel capacity ever closer to the Shannon limit. Some interesting effects are expected to appear if the trend toward wide-band scanning phased array antennas and efficient high-speed modulators continues. For example, in a phased array antenna inter-element spacing, the physical size of the array, and the steering vector can conspire to introduce pulse distortion from group delay, inter-symbol interference, and beam squinting. The phase shifter insertion loss envelope and phase accuracy are also key factors influencing array performance. Phase shifters typically follow low noise amplifiers in a receive array and precede power amplifiers in a transmit array. Since the phase shifter's insertion loss generally depends on its phase setting and since its switching action represents some finite time domain response, its potential contribution to bit error rate degradation cannot generally be ignored. There will always be some effects in any phase-shift keyed (PSK) modulation system, the degree to which depends on the steering vector update rate and data rate. A long switching time also increases minimum radar range. Besides these issues, the satellite communication market's desire to install tracking terminals on commercial mobile platforms, even at small office/home office and residential sites, has inspired the search for inexpensive phase shifters and affordable phased arrays. In practice, system constraints on chip size, power handling, drive

power, insertion loss, bandwidth, phase error, transient response, and cost dictate particular device designs.

24-2 Semiconductor

Semiconductor phase shifters, based primarily on GaAs, but also on SiGe, InP and GaN, have enjoyed steady progress for the past three decades. Their small size and relatively low power consumption compared to ferrite devices has created new insertion opportunities. Many possible circuit topologies, using diode or FET switches in various configurations, exist.

High-Pass/Low-Pass

In principle, any variable reactance in series or shunt across a transmission line can be used to introduce phase shift. A high-pass/low-pass phase shifter π network using discrete capacitors and inductors is shown in Figure 24-1. In the high-pass configuration shown, a relative delay is realized. In the opposite configuration, with all SPDT switches toggled, the low-pass circuit represents a relative phase advance.³ It can be shown that if the circuit is matched, $X=2B/(1+B^2)$ and the insertion phase is $\tan^{-1}(2B/(B^2-1))$.⁴ The switches can be implemented with PIN diodes or MESFETs, which will be discussed later on in this section. It is possible to realize a phase shift of 180° with about 20% bandwidth.

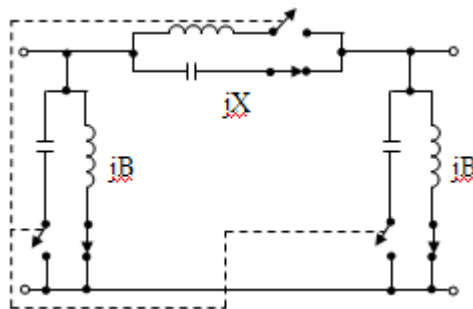


FIG. 24-1. Topology for a high-pass/low-pass π network phase shifter. A dual “T” network realization is also possible.

Loaded Line

Another type of phase shifter generally used for achieving 22.5 to 45 degrees of phase shift is the loaded-line.⁵ A schematic of this is shown in Figure 24-2. Ideally, reactive loads spaced one-quarter wavelength apart are shunted across a transmission line to effect phase shift. The purpose of the second shunt susceptance (jB) is to cause a reflection, which will at least partially cancel the reflection from the first shunt susceptance (jB).

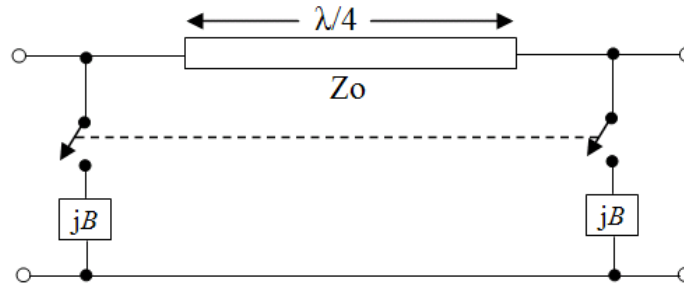


FIG. 24-2. Loaded-line phase shifter

By equating the ABCD matrix of Figure 24-2 to an equivalent section of transmission line with electrical length θ_L radians and characteristic impedance Z Ohms as given in Eq. 1,

$$\begin{pmatrix} 1 & 0 \\ jB & 1 \end{pmatrix} \begin{pmatrix} 0 & jZ_0 \\ j/Z_0 & 0 \end{pmatrix} \begin{pmatrix} 1 & 0 \\ jB & 1 \end{pmatrix} = \begin{pmatrix} \cos(\theta_L) & jZ \sin(\theta_L) \\ j \sin(\theta_L)/Z & \cos(\theta_L) \end{pmatrix} \quad (24-1)$$

we obtain

$$Z = Z_0/[1 - (BZ_0)^2]^{1/2} \quad (24-2)$$

and

$$\theta_L = \cos^{-1}(-BZ_0) \quad (24-3)$$

If the susceptance is capacitive, the phase velocity is decreased; if the susceptance is inductive, the phase velocity is increased. Loaded line phase shifters are inherently narrow-band and produce a constant phase shift versus frequency response. The phase versus frequency response is generally not as flat as the high-pass/low-pass type.

Switched Line

The switched-line phase shifter is yet another popular type, and is intuitively easy to understand. SPDT switches are used to toggle between transmission lines with different path lengths. As opposed to the types discussed previously, this one is a true time-delay device. That is, it provides a phase response (ϕ) proportional to frequency (ω). Since time delay, $\tau = -d\phi/d\omega$ and ϕ is proportional to ω , τ is a constant over the bandwidth. A schematic is shown in Figure 24-3.

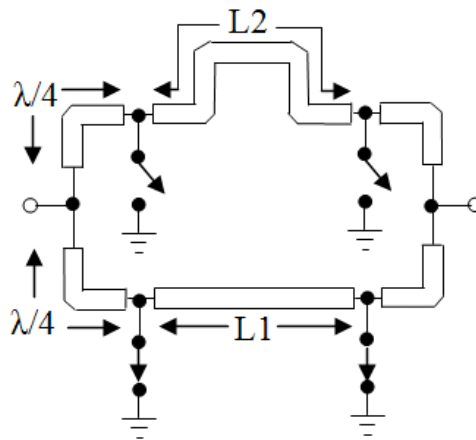


FIG 24-3. Switched-line phase shifter. Signal path is through the delay transmission line with the switches set as shown.

The differential phase shift is

$$\Delta\phi \approx \beta(L2 - L1) \quad (24-4)$$

where β is the propagation constant of the transmission line. As usual, β equals the radian frequency ω divided by v_p , where v_p is the phase velocity. A point of caution needs to be made with regard to this design, however. Utilizing series diode switches, it is possible that the off path length and switch capacitance can conspire to create a through path in parallel with the on path, resulting in high insertion loss and abrupt phase change in band.

A photograph of a GaAs receiver module including a 4-bit monolithic phase shifter is shown in Figure 24-4. The chip size is approximately $5.5 \times 2.5 \times 0.15 \text{ mm}^3$. The 180° , 90° , and 45° bits are implemented using the switched line approach, whereas the 22.5° bit is realized with a loaded line. The operating frequency was 30 GHz with about a 10 percent bandwidth. Average insertion loss was $<10 \text{ dB}$ with an insertion loss envelope of about 2 dB ⁶.

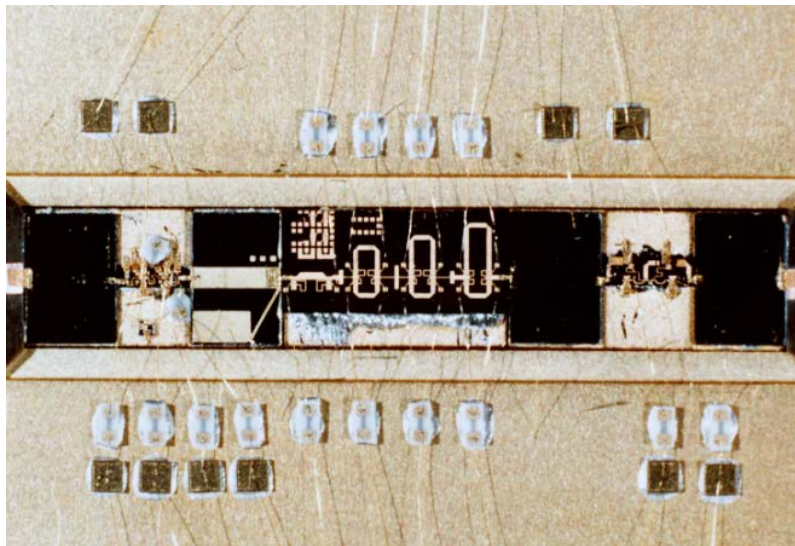


FIG.24-4. 30 GHz GaAs MMIC phased array receiver module (low noise amplifier, 4-bit phase shifter, and gain control amplifier). The Phase shifter uses 1 x 400 μm switching FETs. The phase shifter is $5.5 \times 2.5 \times 0.15 \text{ mm}^3$ not including off-chip capacitors.

Beam Squint

A clear advantage of a constant time-delay is that beam steering is independent of frequency. For simplicity, consider a linear array of N elements separated by distance d .⁷ The

incremental phase shift between adjacent elements to form the beam at an angle θ from boresight is

$$\Delta\phi = (-2\pi d/c) f \sin(\theta) \quad (24-5)$$

where f is frequency and c is the speed of light in vacuum. If the frequency changes by Δf , the beam squint angle $\Delta\theta$ and phase deviation $\delta\phi$ are related by

$$(\Delta\phi + \delta\phi) = (-2\pi d/c) (f + \Delta f) \sin(\theta + \Delta\theta) \quad (24-6)$$

If the phase shifter insertion phase is proportional to frequency, the beam squint $\Delta\theta$ is zero. If the phase is independent of frequency, however, $\delta\phi$ is zero and equations (5) and (6) must be equal, yielding

$$f \sin(\theta) = (f + \Delta f) \sin(\theta + \Delta\theta) \quad (24-7)$$

which causes a beam squint angle

$$\Delta\theta = -\theta + \sin^{-1}[\sin(\theta)/(1 + \Delta f/f)] \quad (24-8)$$

Hence, wide scan angles and wide bandwidths correspond to significant scanning errors. In practice, phase shifters generally provide 0 to 2π phase shift. In electrically large arrays, the integer portion N of total delay required for true-time delay beam steering may be omitted, resulting in degraded performance. In radar systems, where narrow pulses are required for high resolution, there is a correspondingly wide frequency spectrum. The effect of this modulo- 2π problem is considered later in this chapter.

The distribution of amplifier and phase shifter control signals in a large phased array is a complex problem. Thousands of MMIC modules must be interconnected into the beam forming manifold. Some type of digital interface circuitry must be used to address individual phase shifters and decode their control signals. The multiplexed data rate to accommodate fast scanning may approach a Gb/s.⁸ In one instance, a GaAs optoelectronic integrated circuit was used to detect and demultiplex an optical serial control signal into 16 parallel electrical signals.⁹ Operation of a Ka-band, 4-bit phase shifter at 30 MHz clock speeds was demonstrated. Average optical power was 250 μ W. In another instance, optically controlled switching and X-band phase shifting was demonstrated such that the optically controlled GaAs FET interacted directly with the microwave signal.¹⁰ The FET was illuminated by the focused output of a 5 mW, 670 nm, InGaAlP laser diode.

Switching Q

Key requirements for microwave phase shifters include bidirectional (or reciprocal) functionality, low power dissipation, and low insertion loss. The insertion loss of the switched line phase shifter in the previous section depends on the SPDT switch loss and transmission line loss. As we have seen, an SPDT switch can be realized by several possible combinations of SPST switches. Basically, the switch is intended to minimize insertion loss in one state, and maximize isolation in the other. There are two fundamental configurations for SPST switches: as a series impedance or a shunt admittance. These are illustrated in Figure 24-5.

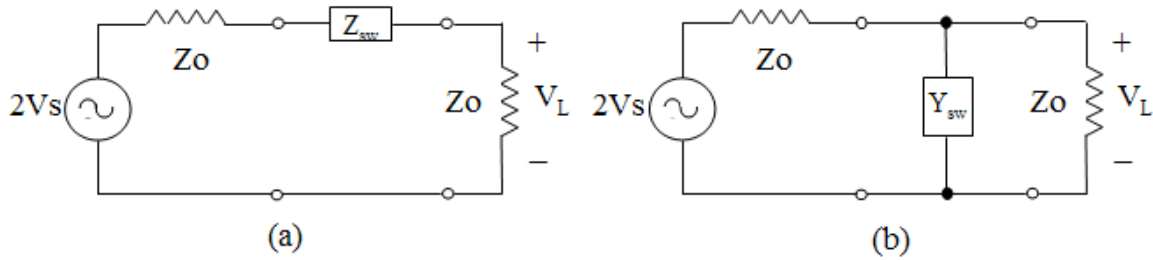


FIG. 24-5. Equivalent circuit for series (a) and shunt (b) single pole, single through switch. The switch impedance and admittance are $Z_{sw}=R_{sw} + jX_{sw}$ and $Y_{sw} = G_{sw} + jB_{sw}$, respectively.

Defining insertion loss as the ratio of available power delivered by the generator to the load in the absence of the switch, to the actual power dissipated by the load in the presence of the switch, the insertion loss for the series (L_{se}) and shunt (L_{sh}) switch is

$$L_{se} = 20 \log \left| 1 + \frac{R_{sw} + jX_{sw}}{2Z_o} \right| \quad \text{dB} \quad (24-9a)$$

$$L_{sh} = 20 \log \left| 1 + \frac{(G_{sw} + jB_{sw})Z_o}{2} \right| \quad \text{dB} \quad (24-9b)$$

In general, Z_{sw} and Y_{sw} , and Z_o for that matter, are frequency dependent. The swing in Z_{sw} and Y_{sw} determine insertion loss and isolation. Of course, the diodes and MESFETS used to realize the switches are inherently nonlinear. Diodes are forward- and reverse-biased, in order to produce the maximum possible change in impedance. In the forward bias state, the impedance is small, but the diodes conduct substantial dc current. In the reverse bias state, a depletion region is formed. It's worth noting that according to well-accepted theories for junction capacitance C_j , as forward bias is increased, C_j grows unbounded. Of course, capacitance is a measure of stored charge, and as the depletion region shrinks towards zero dimension, the stored charge diminishes towards zero.¹¹

GaAs MESFET devices have replaced diodes in many switching applications. Monolithic integration advantages and lower power consumption are incentives. A FET is basically a gate voltage controlled resistor. Insertion loss is largely dictated by channel resistance, and gate-to-source capacitance determines isolation. To increase isolation (high impedance off state), a short (inductive) section of a transmission line is connected between the source and drain to resonate out the pinch-off capacitance C_{off} .^{12,13} Ideal equivalent circuit models for on and off FETs are shown in Figure 24-6.

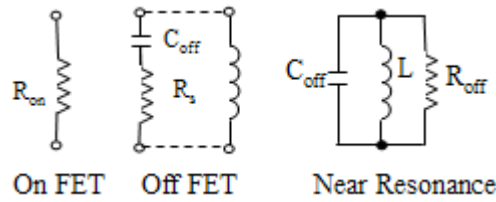


FIG. 24-6 Ideal equivalent circuits for on and off FETs. The inductor L is a short section of a transmission line used to parallel resonate the RC combination in order to enhance the high impedance state.

The resistor R_s is the total series resistance at pinch-off (undepleted channel resistance plus source and drain contact resistance). Sokolov¹³ defined a figure of merit (Q) for switching FETs based on the work of Kurokawa and Schlosser¹⁴ for a device switching between two impedance states Z_1 and Z_2 , such that

$$Q^2 = \frac{|Z_1 - Z_2|^2}{r_1 r_2} = \frac{(R_{on} - R_s) + (\omega C)^{-2}}{R_{on} - R_s} \quad (24-10)$$

Here, r_1 and r_2 are the resistive components of the two impedance states. For the FET switch, $Z_1 = R_{on}$ and $Z_2 = R_s - j(\omega C_{off})^{-1}$. Assuming $(R_{on} - R_s) \ll (\omega C_{off})^{-1}$, a good approximation to Eq. 10 is

$$Q^2 = (R_{on}R_s)^{-1} (\omega C_{off})^{-2} = R_{off}/R_{on} \quad (24-11)$$

Notice that Q degrades as the square of frequency. A high figure of merit requires small R_{on} , R_s , and C_{off} . Scaling the gate width allows a trade off between isolation and insertion loss. If the gate width is doubled, R_{on} and R_s are halved, C_{off} is doubled, and Q is invariant. Typical values of Q^2 at 10 and 30 GHz are about 1000 and 100, respectively. In normal operation, no bias is applied to the drain. A negative bias on the gate (relative to the source) pinches off the channel. Zero or positive gate bias turns the channel on. Additional information on switching Q and its relationship to loss is provided in the reference section.^{15,16}

24.3 Thin Film Ferroelectric

Serious research on bulk (waveguide) ferroelectric phase shifters began in the 1960s but poorer performance in comparison to ferrite devices, coupled with very high tuning voltages, forestalled industrial acceptance. New thin film deposition techniques and novel circuit designs in the 1990s heralded a new generation of devices rivaling their semiconductor counterparts in essentially every figure-of-merit.

Materials and Basic Properties

In a ferroelectric material, such as $Ba_xSr_{1-x}TiO_3$, applying a dc electric field shifts the position of the central Ti atom in the crystal, resulting in a net dipole moment on a macroscopic scale (ionic polarization). Analogous to ferromagnetic materials, domains form in the material where the dipoles are locally aligned (orientational polarization). The Ti ion can remain shifted even after the applied field is removed, and the domains can move in response to applied ac and dc fields. Microwave phase shifters are generally operated above the Curie temperature, in the

paraelectric state. Ideally, this means operating without residual polarization and domain formation, thereby reducing hysteresis and dielectric loss. The Curie temperature, which represents a phase change to a nominally cubic crystal lattice, can be tailored for a specific operating temperature by adjusting the composition of $\text{Ba}_x\text{Sr}_{1-x}\text{TiO}_3$ (BST), where $0 < x < 1$, and for room temperature $x \approx 0.60$. There is interest in ferroelectric-based agile microwave circuits because of their high power handling capability, negligible dc power consumption, and potential for low loss and cost. The ferroelectrics discussed here belong to the perovskite crystal family. The dielectric constant (ϵ_r) of single crystal SrTiO_3 , an incipient ferroelectric, can be depressed from about 20,000 to 2000 with a dc field of 10^4 V/cm at 4.4 K (breakdown voltage for the materials of interest here is $>10^5$ V/cm) and the loss tangent maintained below 0.1%. Thin films of SrTiO_3 exhibit $\tan\delta$ as poor as 0.01 with a peak relative dielectric constant of ≈ 5000 . The dielectric constant also tends to exhibit a broad maximum with temperature as opposed to bulk material. The differences in behavior have been attributed to residual domain wall motion, compositional inhomogeneities, interface layers between the film and electrodes, and lattice mismatch induced stress. Fundamental loss mechanisms have been considered in some situations.¹⁷ Attempts to reduce $\tan\delta$ have included annealing, which tends to increase grain size, and the use of dopants, which may reduce free charge or otherwise affect loss mechanisms.¹⁸⁻²⁰ Several ferroelectric phase shifters have been developed with varying success. A stripline circuit with a BST capacitor provided a differential phase shift of 11° at X-band with a biasing field of 70 kV/cm.²¹ In that same work, a center-wire bias waveguide phase shifter produced more than 360° of phase shift at Ku-band by changing the bias between the wire and waveguide walls from 0 to 2500 V. A planar microstrip phase shifter was reported that provided $20^\circ/\text{kV}$ at 2.65 GHz.²² A phase shift of 165° at 2.4 GHz with only 3 dB loss and a bias of 250 V was obtained from a

microstrip on a thin BST slab synthesized using a sol-gel technique.²³ There was also a 40 GHz phased array antenna that used radiating slots in waveguide and a BST film sintered onto a MgO substrate.²⁴ Voltage applied across a periodic set of electrodes changed the dielectric constant of the BST from 700 to 1500 and a $\tan\delta$ of 0.05 was reported. A ferroelectric lens that uses BST slabs sandwiched between conducting plates was also proposed.²⁵ The approaches advanced thus far have not been able to simultaneously address low cost, low loss, and small size. And in some cases, the impedance variation, due to widely changing permittivity, posed additional difficulties. Two promising implementations include coupled line and synthetic line-based devices, to be discussed next.

Coupled Microstripline

Another style of phase shifter uses coupled microstriplines as dc electrodes to polarize a thin ($\approx 0.4\mu\text{m}$) ferroelectric film. With $\text{YBa}_2\text{Cu}_3\text{O}_{7-\delta}$ electrodes and $2.0\mu\text{m}$ thick SrTiO_3 films, this phase shifter produces a figure of merit approaching $120^\circ/\text{dB}$ at 40 K.²⁶ At room temperature, using Au electrodes and 400 nm thick $\text{Ba}_{1-x}\text{Sr}_x\text{TiO}_3$ films devices have demonstrated $\approx 70^\circ/\text{dB}$.²⁷ These planar phase shifters are fairly compact, low loss, easy to fabricate, and can provide 360° of phase shift with bias voltages under 350 V. Such devices can enhance conventional (direct radiating) phased array performance or enable a new type of reflectarray antenna.^{28,29} Only one control line is required per phase shifter, thereby simplifying array assembly. The power supply does become problematic because of the complex wiring harness distribution (i.e. a central high voltage supply distributed to a large number of individually controlled phase shifters). An alternative architecture uses a low voltage central supply and miniature step-up transformers behind each phase shifter. A piezoelectric transformer-based driver has been developed. The

proof-of-concept circuit achieves voltages in excess of 400 VDC and was used to drive a Ka-band phase shifter.³⁰ A variation in the coupled-line approach was realized with a hybrid X-band device consisting of four cascaded coupled microstrip lines, patterned over 400 nm thick laser-ablated Ba_{0.50}Sr_{0.50}TiO₃ films, followed by a switch.³¹ The ferroelectric section provides (nominally) 180 degrees of analog phase shift. Basically, as a bias from 0 to 350 V is applied across the coupled line electrodes, the relative dielectric constant of the film tunes from about 2000 to 800, thereby modifying the propagation constant. The ferroelectric films are, of course, excellent dielectrics and the current draw is negligible so there is virtually no power consumption. Switching speed for these devices is limited by the external power supply. This is analogous to MESFET switches, wherein there is no drain bias. The variable resistance of a FET switch is a function of the population of majority carriers, as opposed to minority carriers in PIN diodes. (For example, in FET switches, speed is not limited by minority carrier lifetime, but rather the gate control circuitry). The beam lead GaAs diode switch is appended to the last coupled microstrip section and toggles between an open and virtual short circuit, realized with a quarter-wave radial stub. This results in a “digital” transition between a reflection coefficient with magnitude near unity and phase of ≈ 0 degrees and ≈ 180 degrees, respectively. Thus, a full 2π phase shift is possible. The average loss at X-band was 3.2 dB with a 10 % bandwidth. The device is pictured in Figure 24-7. Note that the unmatched beam-lead diode contributed 0.5 to 0.75 dB to the overall insertion loss. In principle, this can be improved by “resonating-out” the diode capacitance.

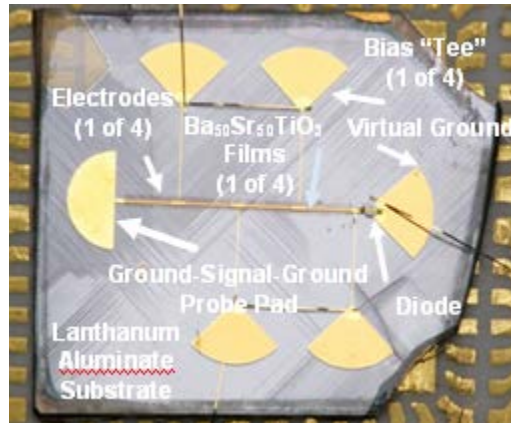


FIG. 24-7. Hybrid X-band ferroelectric/semiconductor phase shifter on 0.5 mm thick lanthanum aluminate. The device measures $\approx 1 \times 1$ cm.

Theory of Coupled-Line Type

A sketch of the cross-section of a coupled-line (multi-dielectric-layer) ferroelectric phase shifter is shown in Figure 24-8. Y_1 and Y_2 represent the admittance looking in the positive and negative y direction, respectively, from the charge plane. The thickness of the ferroelectric layer is h_1 while the host substrate has thickness h_2 .

By concentrating the fields in the odd mode, the phase shift per unit length is maximized and by using the material in thin film form the effects of high loss tangent are reduced.

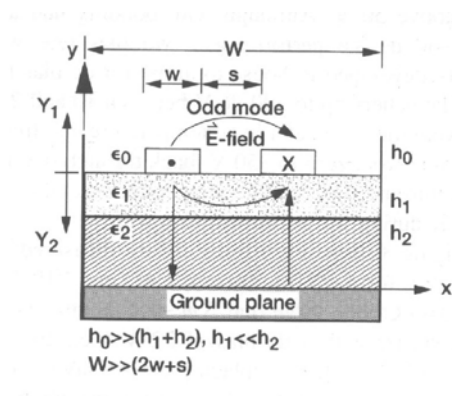


FIG. 24-8. Cross-section of the coupled microstripline phase shifter, showing the odd-mode electric field configuration.

The amount of phase shift can be increased by cascading coupled line sections. Though methods for calculating the propagation parameters of coupled transmission lines are well known, coupled lines on stratified substrates are difficult to analyze. And the high permittivity of the ferroelectric layer causes long computation time by full-wave electromagnetic simulators because the geometry must be fractured into many thousands of cells. The multilayer structure has been analyzed using a computationally efficient variational method for calculating the complex propagation constant and characteristic impedance.³² Space limitation prevents a full description of that work here. However, the method is quite general and can be used for multiple layers of various dielectrics or other types of transmission lines. For example, a multi-layer microstrip can be analyzed by allowing the strip spacing (s) to become much greater than the effective substrate thickness (h) or strip width (w). Minimum loss occurs when current flows through one line and returns through the other (odd-mode), obviating the need for the ground plane. Maximum loss occurs when equal currents flow through the two lines and return through the ground plane (even-mode). Three basic modes are illustrated in Figure 24-9.

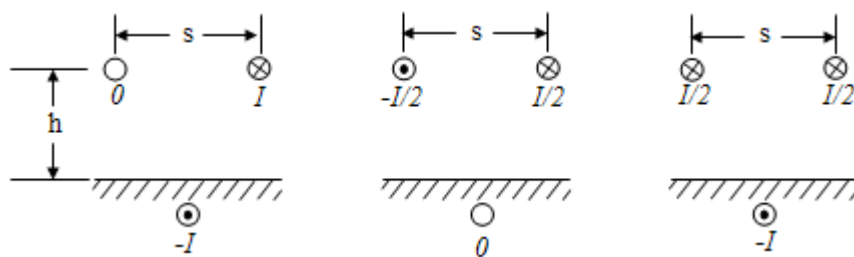


FIG. 24-9. Coupled line modes: microstrip mode (left), $s \gg h, w$; odd-mode (middle); even-mode (right).

Note that the ferroelectric layer thickness is crucial to performance. In principle, the phase shift for a 2 μm thick film is 2.2 times greater than that of a 0.5 μm film. However maintaining the crystalline quality of the pulse laser ablated $\text{Ba}_x\text{Sr}_{1-x}\text{TiO}_3$ films past a thickness of 0.5 μm or so

has proven to be difficult. Experiments have shown that the insertion phase shift is roughly proportional to $h_1^{0.67}$. In the case of cascaded coupled lines, increasing phase shift occurs at the expense of bandwidth since the structure resembles a multi-pole filter. Changing the dielectric constant of the ferroelectric film to change its insertion phase also modifies the pass band characteristic. Operation near band edges is to be avoided since that represents distorted transmission which degrades bit-error-rate performance. The device discussed in the previous section “Coupled Microstripline” helps alleviate this problem. The impedance matrix of the cascade network can be derived by traditional coupled line theory, using the superposition of even and odd mode excitation. Then an equivalent S-parameter model can be extracted and used to predict the pass-band characteristics of the phase shifter. A key advantage of this technology is the relatively large feature size. Active devices at the frequencies of interest here would necessitate submicron gate length GaAs FETs. The finest feature size associated with the coupled-line phase shifters is the electrode separation, typically $\approx 10 \mu\text{m}$. Whereas the GaAs FET performance is largely dictated by transconductance, and hence, carrier transit time across the gate region, the coupled-line phase shifters are static devices. The electrode gap separation determines the degree of electromagnetic coupling and the dc potential required to tune the film.

24.4 MEMS

Micro-electro-mechanical systems (MEMS) can essentially be used to replace PIN diode or FET switches in conventional phase shifters. A typical switch consists of a metal membrane bridge suspended several microns above a lower metal contact. Electrostatic attraction between the flexible membrane and lower contact is used to toggle the switch. A very thin dielectric coating (for example, Si_3N_4) may be used on the lower contact to eliminate a dc path and reduce “stiction,” or a tendency to latch (also known as Van der Waals forces). Larger bridge heights

(gaps) reduce parasitic capacitance, but increase pull-down voltage and may contribute to more fatigue. Typical actuation voltages are between 20 and 100 V. An interesting advantage of MEMS switches is that they do not depend on the characteristics of the substrate. Hence, they may be fabricated on any material that is compatible with standard IC processing. A photograph of one type of MEMS switch is shown in Figure 24-10³³. Optimizing the switching Q amounts to minimizing the parasitic capacitance of the bridge in the off state (bridge up), and maximizing capacitance in the on state (bridge down). When the cantilever is down, the parallel plate capacitance between the metal membrane and the bottom electrode, C_{on} , is large and the switch behaves as a short circuit. Typical ratios of C_{on}/C_{off} are ≈ 100 .

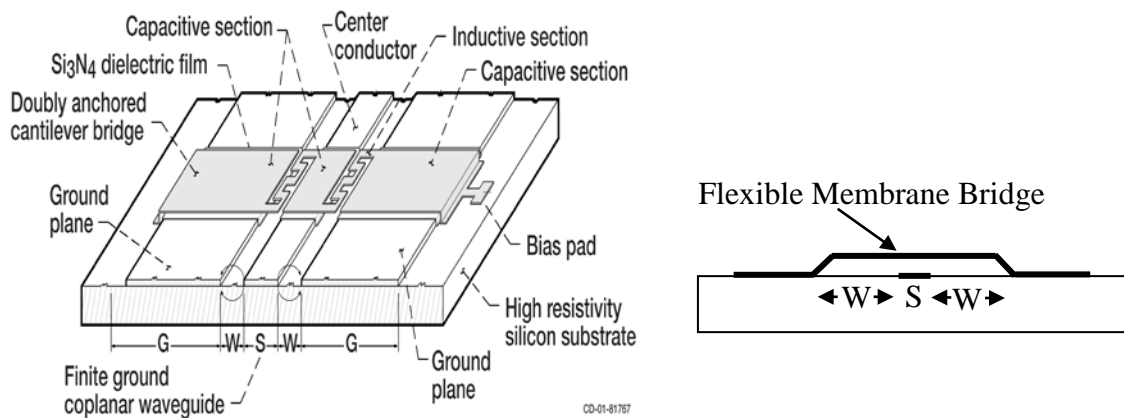


FIG 24-10. RF MEMS capacitive switch. MEMS devices incorporating capacitive/inductive sections allow the switch to be designed for minimum loss and maximum isolation over a wide frequency range (IEEE 2002, Reproduced, with permission, from M. Scardelletti, G. Ponchak, N. Varaljay, “MEMS, Ka-Band Single-Pole Double-Throw (SPDT) Switch for Switched Line Phase Shifters,” *IEEE International Symposium on Antennas and Propagation* (June 2002))

A number of distributed MEMS transmission line phase shifters have been developed.³⁴ An insertion loss of 4 dB at 60 GHz (for a full 360° phase shift) and 257°/dB at 50 GHz has been reported.³⁵⁻³⁶ These excellent results have been obtained from MEMS bridge capacitors placed

periodically along a coplanar waveguide (CPW) transmission line. The theory of such “slow-wave” circuits is discussed in the next section. Activating the MEMS increases the capacitive loading, thereby controlling the insertion phase. A mechanical analysis of operation was provided³⁷ and the bridge spring constant was given as

$$k \approx 32Et^3w/(S + 2W)^3 + 8\sigma(1 - \nu)tw/(S + 2W) \quad N/m \quad (24-12)$$

where E is Young’s modulus of the bridge material, t is the bridge thickness, w is the bridge width, S is the CPW center conductor width, W is the CPW center conductor-to-coplanar ground spacing, σ is the internal residual stress of the bridge, and ν is Poisson’s ratio. The pull-down voltage V_p is given as

$$V_p = [8kg_o^3/(27\epsilon_oSw)]^{1/2} \quad V \quad (24-13)$$

where ϵ_o is the free-space permittivity and g_o is the zero-bias bridge height.

One issue with MEMS phase shifters is that packaging is perhaps more critical than with alternative technologies. Hydrocarbon contamination may compromise MEMS reliability so hermetic seals and careful processing are required. Contact point degradation limits reliability, especially at high power levels. A summary of performance and implications for phased arrays are presented in the reference section.^{38,39} A 3-bit MEMS phase shifter with an average insertion loss of 4.4 dB at 34.75 to 35.25 GHz was recently reported.⁴⁰ The MEMS switch was able to withstand up to 1 W RF power up to 100 million cycles without contact failure.

24.5 Slow-Wave

Periodically loaded transmission lines are used to realize band-pass, slow-wave circuits such that $v_p \ll c$. By using tunable loads or varactors, broad-band phase shifters can be designed.

One-Dimensional Periodic Structures

Consider a cascade of short sections of lossless transmission line shunted by a voltage variable capacitance C' , so as to form the infinite periodic structure illustrated in Figure 24-11. Each distributed transmission line section is modeled by an LC circuit and each unit cell consists of L , C , and C' . Let the separation of each unit cell be designated as s . Such periodic structures exhibit slow-wave behavior ($v_p \ll c$) and band-pass characteristics, like filters. The phenomenon is analogous to acoustic wave propagation in crystal structures. These types of circuits are often referred to as synthetic line, slow-wave, or distributed transmission line phase shifters.

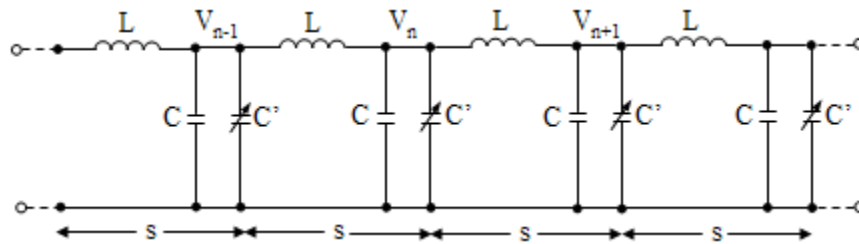


FIG. 24-11. A chain of LCC' circuits representing an infinite, periodically loaded transmission line resulting in slow-wave propagation.

A wave traveling through this periodic structure will only experience a phase shift from unit cell to unit cell, such that V_n is delayed relative to V_{n-1} as

$$V_n = V_{n-1} e^{-j\theta_s} \quad (24-14)$$

In general, θ_s could be complex to account for attenuation as well as phase shift. Summing currents leaving node n

$$0 = V_n(j\omega C + j\omega C') + (V_n - V_{n-1})(-j/(\omega L)) + (V_n - V_{n+1})(-j/(\omega L)) \quad (24-15)$$

Substituting Eq. 12 into Eq. 13 we arrive at

$$\cos(\theta_s) = \frac{1}{2}(2 - \omega^2 L(C + C')) \quad (24-16)$$

Requiring θ_s to be real to represent a propagating mode, letting $\cos(\theta_s) = \pm 1$, we find the structure of Figure 12 has a zero lower frequency cutoff ω_L (obvious by inspection) and an upper cutoff frequency ω_H corresponding to

$$\omega_H = 2/(L(C + C'))^{1/2} \quad (24-17)$$

Since $\theta_s = \beta s$, the insertion phase shift can be approximated knowing the extremes of the tuning range of C' and the number of cascaded sections. Slow wave phase shifters are, in principle, time delay devices (in other words, phase shift is proportional to frequency).

Ferroelectric Varactor

One type of slow wave phase shifter, based on ferroelectric “varactors” is shown in Figure 24-12. Coupled lines, as described in the previous section called “Theory of Coupled-Line Type”, are attached transversely to the propagation direction in a microstrip configuration.⁴¹ A unit cell consists of two microstrip sections, with an intervening orthogonal coupled microstrip line terminated in a virtual open circuit. The open circuit is realized by cascading a nominally quarter-wave high-impedance microstrip line, having impedance Z_p , with a radial stub. The stub provides a very good approximation to a short circuit at its vertex, over almost an octave bandwidth, and the input impedance (Z_{in}) to the combination is approximately $35Z_p/\alpha$, where α

band exhibited an average loss of about 5 and 6 dB, respectively.⁴⁵ One advantage of the parallel plate approach is that conventional tuning voltages can be used (for example, ≈ 10 V as opposed to > 100 V for coplanar structures). Another advantage is that circuits can be fabricated on convenient substrates like Si instead of exotic, high epsilon substrates like LaAlO_3 . Propagation in semiconductor substrates has also been discussed.⁴⁶ The circuits are also extremely compact. A Ku-band version measuring 1×0.8 mm was reported.⁴⁵

Ferroelectric deposition methods (for example pulse laser, sputtering, and so on) require an oxidizing atmosphere around 700°C to achieve high quality crystalline films. Hence, electrodes for parallel plate varactors, as opposed to the coplanar or interdigital structures described previously, must be impervious to high temperature oxidizing atmospheres. Low dielectric constant oxides at the electrode interface can drop most of the electric field and substantially reduce tuning. Pt is a popular electrode material choice.

24.6 Ferrite

The fundamental source of a material's magnetic properties is the magnetic dipole moment associated with what is visualized as an electron spinning about its axis. In non-magnetic materials, the number of electrons with up spins and down spins is equal, so the net magnetic moment is negligible. In a magnetic material, one variety dominates and can be aligned by an external DC magnetic bias field H to generate a large magnetic moment, as long as thermal fluctuations aren't too strong. The spin magnetic moment vector precesses about the H-field vector at an angular frequency $\omega_m = 2\pi f_m$. Precession sense (i.e. polarization) depends on the direction of H . The precession frequency is proportional to H such that $f_m = \gamma H$, where $\gamma = 2.8$ MHz/Oe is the gyromagnetic constant. The propagation constant (β) in a ferromagnetic medium is

$$\beta \approx (2\pi \text{Error! Bookmark not defined. } \sqrt{\varepsilon \mu'}) / \lambda$$

(24-18)

where μ' is the real part of the permeability and ε is the dielectric constant of the ferrite. When the frequency f of a microwave magnetic field equals f_m , ferrimagnetic resonance occurs. This is the underlying cause for opposite circularly polarized waves experiencing different permeabilities, μ'_+ and μ'_- . In the absence of any loss mechanism, the material's susceptibility would become infinite at the gyromagnetic resonance frequency. The permeability can be tuned by changing M , which is the magnetization or magnetic moment. As the strength of the magnetic bias field increases, M will reach an upper limit called the saturation magnetization, denoted as M_s . Ferrite materials tend to have high loss below saturation at microwave frequencies. The choice of ferrite for a particular application is determined by selecting $\gamma 4\pi M_s$ sufficiently below the operating frequency f . When f_m is small compared to f , there is a significant difference between μ'_+ and μ'_- for the two polarization senses. (Recall that a linearly polarized wave can be disassociated into two counter-rotating circularly polarized components). With this condition, it can be shown that⁴⁷

$$\mu'_{\pm} = 1 \mp \gamma 4\pi M / f \quad (24-19)$$

and the corresponding phase shift is

$$\Delta\phi = 2\pi \sqrt{\varepsilon} [(\mu'_+)^{1/2} - (\mu'_-)^{1/2}] L / \lambda \quad (24-20)$$

where L is the length of the ferrite section. In practice, the phase shift is implemented by reversing the direction of the magnetization vector.

As was alluded to in the introduction, ferrite phase shifters have tended to dominate the phased array landscape. The basic, nonreciprocal, latching phase shifter consists of a toroidal

ferrite core in a section of waveguide. A drive wire passes through its center, which is used to magnetize the material. At this point it becomes latched at one of two remanent states, depending on the polarity of the bias. The amount of differential phase shift between the two states is determined by the toroid length. Another common device is the reciprocal, non-latching Reggia-Spencer phase shifter. A ferromagnetic bar is located axially in a section of waveguide, which is wound by a solenoid. The solenoid produces a longitudinal magnetic field that changes the permeability of the bar material. The performance of twin-toroid, dual-mode, and rotary-field ferrite phase shifters has been discussed elsewhere.⁴⁸ A proof-of-concept magnetically tunable split-mode device based on magneto-dielectric resonance in yttrium iron garnet (YIG) was recently demonstrated at W-band. A phase shift of 30 degrees with 1.5 dB of insertion loss was reported using a tuning field of 1600 Oe.⁴⁹

24.7 Effect of Phase Shifter Behavior on Phased Array Bit Error Rate

Phase shifters' phase errors can cause some signal distortion, and phase transients can cause beam pattern degradation during direction switching. Signal models have been established for both static and transient cases. Moreover, modulo 2π effects cause intersymbol interference (ISI).

Modulo 2π Effects

The composite far-field signal formed by a phased array is the summation of individual contributions from each elemental radiator. Radiation path lengths to the far-field observation point are different for each elemental radiator on the array surface. To form a co-phasal beam, modulo- 2π compensation is provided by the phase shifters. Integer-multiples of 2π are generally not provided, and for an electrically large array, this leads to inter-symbol interference (ISI) in

phase-shift keyed modulation formats. The ISI is formed because different delays from each signal component destructively interfere. ISI results in composite (total) signal amplitude loss at the symbol boundary. As an example, for a reflectarray^{28,29} operating at $f = 26.5$ GHz with a bit rate of 1.325 Gbps, the BER degradation due to ISI is proportional to the symbol rate and the loss ranges are from about 1 dB to around 2 dB in E_b/N_o , depending on original E_b/N_o , for BPSK, QPSK, 8PSK, and 16QAM.⁵⁰

Phase Errors

Each phase shifter assigned to each element is designed to shift the signal phase by an amount determined by the steering angles of the antenna. In practice, however, there are errors in the phase shifters. Assume that the phase errors are uniformly distributed in $[-\Delta\varphi_{\max}, \Delta\varphi_{\max}]$. It can be shown in that the averaged effect of phase error is to introduce an amplitude loss of

$$L_{\Delta\varphi} = \frac{\sin \Delta\varphi_{\max}}{\Delta\varphi_{\max}} \quad \text{or} \quad L_{\Delta\varphi}(\text{dB}) = \left| 20 \log \left| \frac{\sin \Delta\varphi_{\max}}{\Delta\varphi_{\max}} \right| \right| \quad (24-21)$$

and there is no net phase shift of the composite signal due to the phase errors.⁵⁰ For a maximum phase error of $\pi/8$, the loss is only 0.224 dB. It can be seen that the phase error loss is a sinc function of $\Delta\varphi_{\max}$ and it can be shown that the maximum phase error must be less than 47° to limit the loss within 1 dB.

The real composite signal will have not only amplitude loss, but possibly also a small net phase error. The small net phase error could have a degrading impact on the BER performance of the high-order PSK schemes and QAM schemes, since the phase differences between constellation points are very small. Electrically large phased arrays communicating wide-band signals with high order modulation formats must be designed to compensate for these effects.⁵¹

A set of BPSK BER curves for various conditions is shown in Figure 24-13 (transient effect excluded). The term “without antenna” means that the antenna is ideal—no phase errors and no ISI.

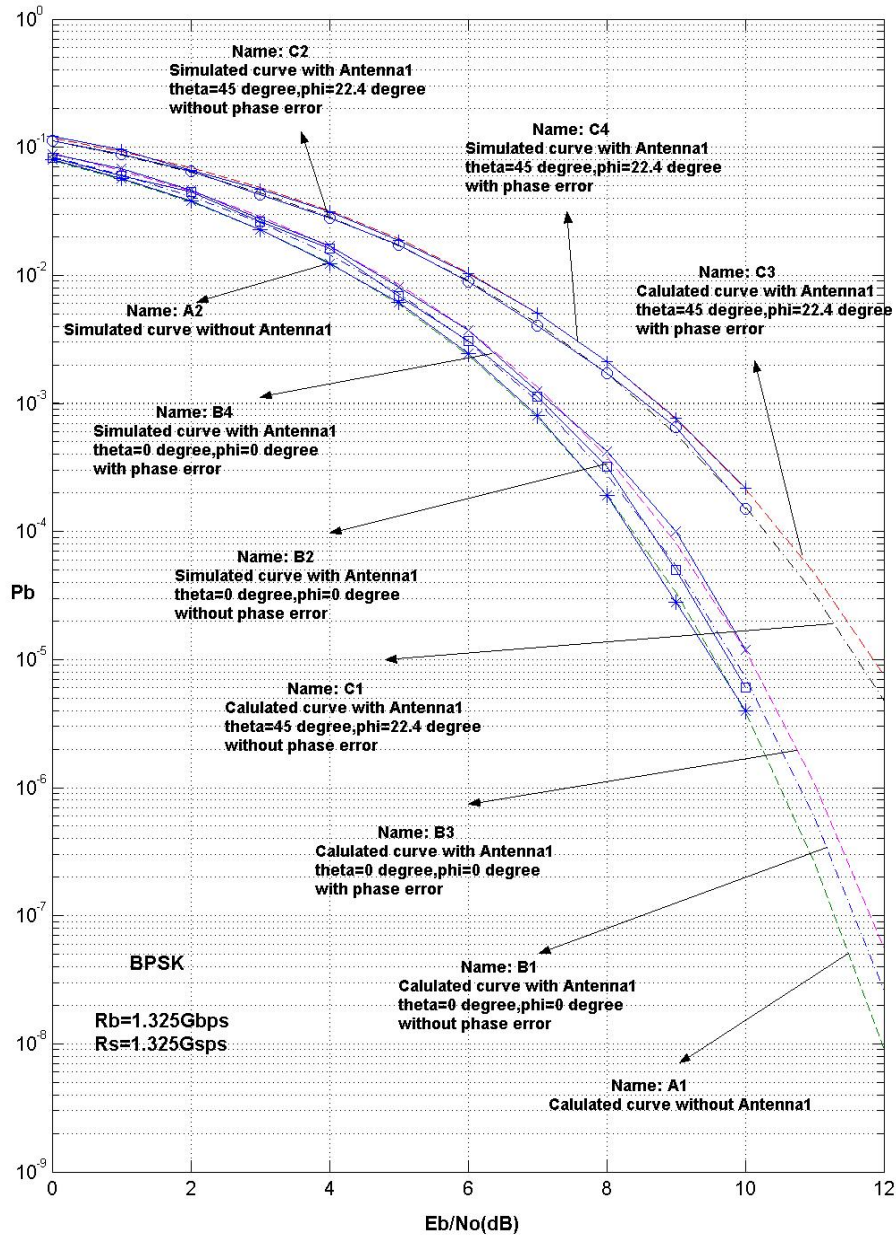


FIG. 24-13. BER curves for BPSK (IEEE 2005, Reproduced, with permission from Xiong and R. Romanofsky, “Study of Behavior of Digital Modulations for Beam Steerable Reflectarray Antennas,” *IEEE Trans. Ant. and Prop.*, vol. 53, No. 3 (March 2005): 1083–1096).

24.8 Trends

Besides the advent of “new” semiconductor materials such as GaN, and progress in ferroelectric and MEMS technology, several interesting developments are underway. These trends may offer additional applications for phase shift technology, and enable new techniques to produce phase shifters.

Optical Phased Arrays

Free-space optical communications has leveraged advancements in the fiber-optic industry and experienced tremendous success in the past decade - spurred by inherent security advantages, unregulated spectrum, and extremely wide bandwidth. Optical phased arrays are analogous to microwave phased arrays and provide an alternative to gimbaled free-space communications links. They can, in principle, also be used to compensate for atmospheric turbulence in imaging systems. Deliberate illumination tapering, to reduce side-lobes, is generally not required since the input optical beam usually has a Gaussian spatial profile. Any technique to introduce a linear gradient of path delay across the aperture will tilt the phase front and effectively steer the beam. Under zero field, liquid crystal molecules orient parallel to an alignment layer at the transparent substrate interface. Applying a relatively low voltage (< 10 V) reorients the molecules and changes the index of refraction. The relative phase shift is proportional to the liquid crystal layer thickness “ t ”. An optical beam polarized parallel to the long axis of the molecules experiences an extraordinary index of refraction n_e . When a sufficient voltage is applied to the nematic-phase (threadlike) liquid crystal films, the molecules align with the field thereby modifying the refractive index to approach the ordinary index n_o . The differential phase shift $\Delta\phi$ between these two states is:

$$\Delta\phi = 2\pi (n_e - n_o) t/\lambda_o \quad (24.22)$$

where λ_o is the free space wavelength. Relaxation time is a function of wavelength and is on the order of 1 ms at the typical communications wavelength (1.55 μm).⁵² Ferroelectric liquid crystals are inherently faster.

A prototype liquid crystal based terahertz phase shifter using graphene films as transparent electrodes has been developed.⁵³ Graphene is of interest to the microwave engineering community because the mobility can be as high as 250,000 cm^2/Vs , leading to high electrical conductivity. Plus, graphene is essentially transparent at visible and terahertz frequencies. At 1 THz, a phase shift of 10.8 degrees at the saturation voltage of 5 V, using a 50 μm liquid crystal cell, was measured. 4-Cyano-4'-pentylbiphenyl is a commonly used nematic liquid crystal. The phase shift can be increased by using materials with larger birefringence, and the phase shift will increase at higher frequencies per equation 22.

Multiferroics

Ferromagnetism, ferroelectricity, and ferroelasticity are the three basic types of ferroic behavior. The term multiferroic is commonly used in reference to materials that exhibit electric field control of permeability, or conversely, magnetic field control of permittivity. The prospect of exploiting voltage-controlled magnetism in microwave systems is gaining traction.⁵⁴ Compared to conventional magnetic-field tunable microwave devices, these dual E- and H- field tunable multiferroic devices promise higher efficiency, smaller size and weight, and faster response times. A proof-of-concept C-band phase shifter based on nonlinear control of spin-electromagnetic waves propagating in a yttrium iron garnet/barium strontium titanate bilayer has been demonstrated⁵⁵. A phase shift of 250, 330 and 180 degrees was effected by signal power, E-field, and H-field, respectively. An electric field tunable multiferroic phase shifter using a

YIG/PbMgTaO-PbTiO heterostructures, also at C-band, has been reported.⁵⁶ The device exhibited a differential phase shift of 119 degrees with an electric field of 11 kV/cm (with no external magnetic field).

Printable Phase Shifters

Using techniques such as inkjet printing, it is possible to combine flexible electronics manufacturing with microwave device design to realize low-cost, lightweight, conformal antenna systems on flexible substrates such as kapton. A flexible 4x4 element C-band phased array has been demonstrated⁵⁷. The phase shifters are enabled by 64 carbon nanotube (CNT) thin-film transistors. The carbon-nanotube FET switches exhibited an on–off ratio of over 1000. Mobilities as high as 100,000 cm²/Vs have been reported for carbon-nanotube material.⁵⁸ The source and drain electrodes of the transistor are printed on top of the substrate, with thickness varying from hundreds of nanometers to a few micrometers depending on the material, printer nozzle size, and resolution. The electrode materials include conductive silver fluids, conductive copper fluids, and conductive polymers.⁵⁹ The CNT layer is printed on top of the electrode layer. A maximum elevation steering angle $\theta = 34$ degrees was chosen to minimize complexity and keep the array within the printable limit.

24.9 Summary

This chapter reviewed basic phase shifter theory and described some modern phase shifter devices. Key developments of the past few decades or so include devices based on semiconductor MMIC, MEMS, and thin ferroelectric films. Some interesting effects are expected to manifest themselves as the ratio of signaling bandwidth to carrier frequency decreases, especially with regard to electrically large phased arrays. A summary of phase shifter characteristics is presented in Table 24-1. New materials such as graphene and multiferroic

approaches may help the technology to achieve superb performance. And new manufacturing techniques, especially printing thin conductive films and carbon nanotubes, may help to dramatically reduce manufacturing costs.

Table 24-1. Comparison of Phase Shifter Technologies

Type Feature	Ferroelectric	Semiconductor/ MMIC	Ferrite	MEMS
Cost	Low	Expensive	Very expensive	Low
Reliability	Good after 10^6 0-40 V/ μm bias cycles (more tests required)	Very good (if properly packaged)	Excellent	Good after several billion cycles (more tests required)
Power handling	Good, >1W	Very good, tens of watts	Very high (kW)	Low Power, <100 mW for high reliability
Switching speed	Intrinsically fast ($\approx\text{ns}$), controller limited if high voltage	Fast at low power ($<10^{-9}\text{s}$)	Slow (inductance) 10 to 100 μs	Slow (mechanical) 10 to 100 μs
Radiation tolerance	Excellent	Poor (good if radiation hardened)	Excellent	Excellent (mechanical; no solid state junctions involved)
DC power consumption	Low ($\ll 1 \mu\text{A}$ current) μW	Low ($< 10 \text{ mW}$ for diodes; negligible for FETs)	High (large current) $\approx 10 \text{ W}$ ($\approx 1 \text{ W}$ if latching)	negligible
RF loss	$\sim 2.5\text{dB}/320^\circ$ @ X-band	$\sim 2 \text{ dB/bit}$ @ Ka-band = 8 dB	$< 1 \text{ dB} / 360^\circ$ @ X-band	$\sim 2.3 \text{ dB}/337.5^\circ$ @ Ka-band
Size	Very small if parallel plate varactor (mm^2)	Small ($\approx 10 \text{ mm}^2$ at Ka-band)	Large (wave-guide, bias coil)	Small (comparable to MMIC)
Linearity	IMD intersect +60 dBm	IMD intersect +35 to +40 dBm (46 dBm GaN ⁶⁰)		IMD intersect +80 dBm

References

1. P.L. Lowbridge, "Low Cost Millimeter-Wave Radar Systems for Intelligent Vehicle Cruise Control Applications," *Microwave Journal*, October 1995, pp. 20-33.
2. <http://www.autonews.com/article/20141013/OEM06/310139961/demand-skyrockets-for-collision-avoidance-sensors>
3. L. Dunleavy, "GaAs MMICs Perform in Phase Shifters," *Microwaves & RF* (April 1984): 49–52.
4. J. White, *Microwave Semiconductor Engineering*, (New York: Van Nostrand Reinhold Co., 1982).
5. G. Bartolucci, F. Giannini, and E. Limiti, "On the Generalized Loaded-Line Phase Shifter," *IEEE Int'l Microwave and Optoelectronics Conf. Proc.* (1995): 554–558.
6. J. Geddes, et al., "Characteristics of 30 GHz MMIC Receivers for Satellite Feed Array Application," *GaAs IC Symposium Digest*, (1987).
7. S. Ohmori, S. Taira, and M. Austin, "Beam Scanning Error of Phased Array Antenna," *Journal of Communications Research Laboratory*, vol. 38, no. 2, (July 1991) 217–222.
8. Z. Wang et al., "Single-Chip 4 Bit 35 GHz Phase-Shifting receiver with a Gb/s Digital Interface Circuitry," *GaAs IC Symposium* (1995): 234–237.
9. K. Bhasin et al., "Control of a GaAs Monolithic Ka-Band Phase Shifter Using a High-Speed Optical Interconnect," *IEEE Trans. MTT* 38, no. 5 (May 1990): 686–688.
10. S. Rossek and C. Free, "Optically Controlled Microwave Switching and Phase Shifting Using GaAs FET's," *IEEE Micro. Guided Wave Letter*, vol. 5, no.3 (March 1995): 8–83.
11. R. Romanofsky, "On the Relationship Between Schottky Barrier Capacitance and Mixer Performance at Cryogenic Temperatures," *IEEE Micro. Guided Wave Letter*, vol. 6, no. 8 (August 1996): 286–288.
12. W. McLevige and V. Sokolov, "Resonated GaAs FET Devices for Microwave Switching," *IEEE Trans. Elect. Dev.*, vol. ED-28, no. 2 (February 1981): 198–204.
13. V. Sokolov, et al., "A Ka-band GaAs Monolithic Phase Shifter," *IEEE Trans. Microwave Theory Tech*, vol. MTT-31, no. 12 (December 1983): 1077–1082.
14. K. Kurokawa and W. Schlosser, "Quality Factor of Switching Diodes for Digital Modulation," *Proc. IEEE*, vol. 38 (January 1970): 180–181.
15. H. Atwater and R. Sudbury, "Use of Switching Q in the Design of FET Microwave Switches," *IEEE MTT-S Int. Microwave Symposium Digest*, (June 1981): 370–372.
16. M. Schindler and A. Morris, "DC-40 GHz and 20-40 GHz MMIC SPDT Switches," *IEEE Trans. Micro. Theory Tech*, vol. MTT-35, no. 12 (December 1987): 1486–1492.
17. A. Tagantsev, "Mechanisms of Dielectric Loss in Microwave Materials," *Materials. Research Society Proceedings*, 603, (2000): 221–232.
18. R. Katiyar, et al., "Investigations on Sol-Gel Derived $\text{Ba}_{0.5}\text{Sr}_{0.5}\text{Ti}_{1-\delta}\text{Mn}_{\delta}\text{O}_3$ Thin Films for Phase Shifter Applications," *Materials. Research Society Proceedings*, vol. 720 (2002): 3–14.
19. H. Wu and F. Barnes, "Doped $\text{Ba}_{0.6}\text{Sr}_{0.4}\text{TiO}_3$ Thin Films for Microwave Device Applications at Room Temperature," *Integrated Ferroelectrics*, vol. 22 (1998): 291–305.
20. N. Navi, J. Horowitz, H. Wu, and S. Qadi, "Structure-Property Relationships in W Doped (Ba,Sr)TiO₃ Thin Films Deposited by Pulsed Laser Deposition on (001) MgO," *Materials. Research Society Proceedings*, vol. 720 (2002); 41–48.
21. V. Varadan et al., "Ceramic Phase Shifters for Electronically Steerable Antenna Systems," *Microwave Journal*, (January 1992): 116–127.
22. V. Varadan et al., "A Novel Microwave Planar Phase Shifter," *Microwave Journal*, (April 1995): 244–253.

23. F. DeFlaviis, N. Alexopoulos, and O. Stafsudd, "Planar Microwave Integrated Phase Shifter Design with High Purity Ferroelectric Material," *IEEE Trans. MTT*, vol. 45, no. 6 (June 1997): 963–969.
24. O. Vendik, I. Mironenko, and L. Ter-Martirosyan, "Superconductors Spur Applications of Ferroelectric Films," *Microwaves & RF* (July 1994): 67–70.
25. J. Rao, D. Patel, and L. Sengupta, "Phased Array Antennas Based on Bulk Phase Shifting with Ferroelectrics," *Integrated Ferroelectrics*, vol. 18 (1998).
26. F. Van Keuls, et al., "YBa₂Cu₃O_{7-δ}, Au/SrTiO₃/LaAlO₃ Thin Film Conductor/Ferroelectric Coupled Microstripline Phase Shifters for Phased Array Applications," *Applied Physics Letter*, vol. 71 (November 1997): 3075–3077.
27. F. Van Keuls, et al., "Ku-Band Gold/ Ba_xSr_{1-x}TiO₃/LaAlO₃ Conductor/Thin Film Ferroelectric Microstripline Phase Shifter for Room Temperature Operation," *Microwave and Optical Tech. Letter*, vol. 20 (January 1999): 53–56.
28. R. Romanofsky, "Advances in Scanning Reflectarray Antennas Based on Thin Ferroelectric Film Phase Shifters," *Proc. IEEE, Special Issue on Technical Advances in Deep Space Communications and Tracking*, Vol. 95, No. 10, pp. 1968-1975 (Oct. 2007)
29. R. Romanofsky et al., "K-band Phased Array Antennas Based on Ba_{0.60}Sr_{0.40}TiO₃ Thin-Film Phase Shifters," *IEEE Trans. MTT*, vol. 48, no. (December 2000): 2504–2510.
30. A. Roberts and R. Romanofsky, "Implementing a Piezoelectric Transformer for a Ferroelectric Phase Shifter Circuit", *Integrated Ferroelectrics*, Volume 134, Issue 1, pp. 102-110 (April 20, 2012).
31. R. Romanofsky, "Broadband, Low-Loss K- and Ka-Band Phase Shifters Based on Thin Ferroelectric Films," *IEEE MTT Symposium Workshop WMC* (June 2004).
32. R. Romanofsky and A. Qureshi, "A Model for Ferroelectric Phase Shifters," *IEEE Trans. Mag.*, vol. 36, no. 5 (September 2000): 3491–3494.
33. M. Scardelletti, G. Ponchak, N. Varaljay, "MEMS, Ka-Band Single-Pole Double-Throw (SPDT) Switch for Switched Line Phase Shifters," *IEEE International Symposium on Antennas and Propagation* (June 2002).
34. G. M. Rebeiz, *RF MEMS Theory, Design, and Technology*, (New York: John Wiley & Sons Inc., 2003).
35. B. Lakshminarayanan and T. Weller, "Design and Modeling of 4-bit Slow-Wave MEMS Phase Shifters," *IEEE Trans. MTT*, vol. 54, no. 1 (2006): 120–127
36. N. Barker and G. Rebeiz, "Optimization of Distributed MEMS Phase Shifters," *IEEE MTT-S Digest* (1999): 299–302.
37. N. Barker and G. Rebeiz, "Distributed MEMS True-Time Delay Phase Shifters and Wide Band Switches," *IEEE Trans. MTT*, vol 46, no. 11 (1998): 1881–1890.
38. M. Scardelletti et al., "RF MEMS Phase Shifters and Their Application in Phased Array Antennas". *IEEE Wireless and Microwave Technology Conference* (April 2005).
39. G. Rebeiz, G-L Tan, and J. Hayden, "RF MEMS Phase Shifters: Design and Applications," *IEEE Microwave Magazine* (June 2002): 72–82.
40. S. K. Koul, et al., "Ka-Band Reliable And Compact 3-Bit True-Time-Delay Phase Shifter Using MEMS Single-Pole eight-Throw Switching Networks," *Journal of Micromechanics and Microengineering*, Vol. 26, 2016.
41. R. Romanofsky, "Slow-Wave Phase Shifters Based on Thin Ferroelectric Films, for Reflectarray Antennas," *IEEE MTT Symposium Workshop WMG* (June 2006): 121-137.
42. A. Nagra and R. York, "Distributed Analog Phase Shifters with Low Insertion Loss," *IEEE Trans. MTT*, vol.47, no. 9 (September 1999): 1705–1711.
43. E. Erker, et al., "Monolithic Ka-Band Phase Shifter Using Voltage Tunable BaSrTiO₃ Parallel Plate Capacitors," *IEEE Microwave and Guided Wave Letter*, vol. 10, no. 1 (January 2000): 10–12.
44. B. Acikel et al., "A New High Performance Phase Shifter Using Ba_xSr_{1-x}TiO₃ Thin Films," *IEEE Microwave and Wireless Comp. Letter*, vol. 12, no. 7 (July 2002): 237–239.
45. R. York, "BST Technology for RF Front Ends," *MTT Symposium Workshop WMG* (June 2006): 73–91.

46. G. Ponchak, "RF Transmission Lines on Silicon Substrates," *29th European Microwave Conference* (October 1999): 158–161.
47. G. F. Dionne et al., "Superconductivity for Improved Ferrite Devices," *Lincoln Laboratory Journal*, vol. 9, no. 1 (1996): 19–31.
48. W. Hord, "Microwave and Millimeter-Wave Ferrite Phase Shifters," *Microwave Journal, State of the Art Reference* (1989): 81–94.
49. M.A. Popov, I.V. Zavislak, and G. Srinivasan, A Magnetic Field Tunable Yttrium Iron Garnet Millimeter-Wave Dielectric Phase Shifter: Theory and Experiment, *Progress in Electromagnetics Research C*, Vol. 25, pp. 145-157 (2012).
50. F. Xiong and R. Romanofsky, "Study of Behavior of Digital Modulations for Beam Steerable Reflectarray Antennas," *IEEE Trans. Ant. and Prop.*, vol. 53, No. 3 (March2005): 1083–1096.
51. R. C. Reinhart, et al., "Phased Array Antenna-based System Degradation at Wide Scan Angles", IEEE International Symposium on Phased Array Systems and Technology, Revolutionary Developments in Phased Arrays, Boston, MA, October 2003.
52. Optical Phased Array Technology," P.F. McManamon et al., *Proc. IEEE*, Vol. 84, No. 2, pp. 268-298, Feb. 1996.
53. Y. Wu et al., "Graphene/Liquid Crystal Based Terahertz Phase Shifters," *Optics Express*, Vol. 21, No. 18, (September 2013).
54. Subramanyam, G. et al., "Challenges and Opportunities For Multifunctional Oxide Thin Films For Voltage Tunable Radio Frequency/Microwave Components," *Journal of Applied Physics* 114(19), 191,301 (2013)
55. A.B. Ustinov, B.A. Kalinikos, and G. Srinivasan, "Nonlinear Multiferroic Phase Shifters For Microwave Frequencies," *Applied Physics Letters* , Vol. 104, (2014)
56. X. Yang et al., "Voltage Tunable Multiferroic Phase Shifter with YIG/PMN-PT Heterostructure," *IEEE Microwave and Wireless Components Letters*, Vol. 24, NO. 3, pp. 191-193 (March2014).
57. H. Subbaraman et al., "Inkjet-Printed Two-Dimensional Phased-Array Antenna on a Flexible Substrate," *IEEE Antennas and Wireless Propagation Letters*, Vol. 12, pp. 170-173 (2013).
58. T. Durkop, S. A. Getty, E. Cobas, and M. S. Fuhrer, "Extraordinary Mobility in Semiconducting Carbon Nanotubes," *Nano Lett.*, vol. 4, pp.35–39 (2004).
59. M.Y. Chen et al., Conformal Ink-Jet Printed C-Band Phased-Array Antenna Incorporating Carbon Nanotube Field-Effect Transistor Based Reconfigurable True-Time Delay Lines," *IEEE Transactions On Microwave Theory and Techniques*, Vol. 60, No. 1, pp. 179-184 (January 2012).
60. T.N. Ross et al., "Design of X-Band GaN Phase Shifters," *IEEE Transactions on Microwave Theory and Techniques*, Vol. 63, No. 1, pp. 244-255 (January 2015)